A UNIQUE POTENTIAL TO STUDY SCATTERING AND FUSION PHENOMENA IN HEAVY ION COLLISIONS AROUND COULOMB BARRIER

Abstract

To examine angular variation in cross-sections of elastic scattering, a systematic recursive formula is developed involving partial-wave scattering matrix for total effective complex potential of nucleus-nucleus collisions. We express cross-sections for the absorption from arbitrary and small intervals in an additional manner. This results in an assessment of the effective potential's absorption contributions in the interior region, which explains fusion cross section (σ_{fus}) data for different incident energies. The interaction potential taken into account in this study is energy-independent and enables states of different partial-wave trajectories owing to its weakly absorbing characteristic. Therefore, it becomes clear that the appearance of these resonance states is the physical cause of the observable oscillatory structure in the modification of the quantity $D(E_{c.m.})$, the second derivative of the product "$E_{c.m.}\sigma_{fus}$" with respect to $E_{c.m.}$. In this chapter, we discuss simultaneous and extremely effective descriptions of the crosss-ections for fusion, elastic scattering, and the outcomes of $D(E_{c.m.})$ in various kinds of heavy-ion collisions.

Keywords: Variation in cross-sections of elastic scattering, the second derivative of the product "$E_{c.m.}\sigma_{fus}$" with respect to $E_{c.m.}$. $D(E_{c.m.})$

Authors

Bidhubhusan Sahu
Department of Physics
School of Applied Sciences
KIIT Deemed to be University
Bhubaneswar, India.
bbsahufpy@kiit.ac.in

Kamala Kanta Jena
P. G.
Department of Physics
Bhadrak Autonomous College
Bhadrak, India.
kkjena1@gmail.com,

Santosh Kumar Agarwalla
P. G.
Department of Physics
Fakir Mohan University
Balasore, India
san1612@rediffmail.com

I. INTRODUCTION

There have been numerous experiments on the nucleus-nucleus collision process, and extensive data on the angular distribution of the elastic scatterings ($\frac{d\sigma(\theta)}{d\sigma_R(\theta)}$) for various energies of incidence and the fusion cross-sections at firmly energy intervals are now available [1]-[5]. Eight such systems come to mind in this regard: $^{12}C+^{208}Pb$ in Refs. [1, 3],$^{16O}+^{208}Pb$ in Refs. [2, 4],$^{19}F+^{208}Pb$ in Refs.[6,7],$_{16}O+_{144}Sm$ in Refs.[8–10],and $_{16}O+_{62}Ni$ in Refs.[11,12] all of which include a wealth of information. The shape resonances, though present, are not observed experimentally in heavy ion systems. But the case is different for the systems with light ions, where the resonances are generated by the effective potential [13]. Further research is needed to ascertain the potential impact and expression of resonances in any other visible forms throughout collision. One employs the phenomenological potential, which is often complicated, to analyse these heavy ion collision data. The observed values of cross section in the elastic scattering at different incident energies are reproduced to determine all the parameters defining the potential. One has to explain fusion cross-section (σ_{fus}) data obtained from fusion process and the phenomena of resonance taking place in the elastic scattering process by using the same interaction potential. It is thus challenging to device a special potential that can address both of these phenomena at the same time. It is because scattering process is surface-sensitive, whereas, fusing process volume-sensitive. The scattering is associated with potential's nature on surface region, but fusion is an internal activity. Once we obtain data from elastic scattering for theoretical analysis, the results of total reaction cross section (σ_r) can be found easily. Total cross-section is the sum of cross sections for various reaction channels, in which the fusion channel predominates in low-energy collisions. It is difficult to separate the part of reaction cross section from the total value that is an exact amount of the measured data of σ_{fus}.

The cross-section σ_r is taken into account in the scope of the optical potential model analysis of scattering by the expected value of the imaginary component of the potential, calculated using the distorted waves from the full potential in the elastic channel. This is just the sum of the cross-sections produced by absorption in all of the potential's different regions where the imaginary portion is present. We can use the same wave function as used to explain the elastic scattering data to obtained the absorption cross-section $\boldsymbol{\sigma_i^A}$ in ith infinitesimally small ith radial interval $\mathbf{\delta r_i}$ so that the total absorption cross-section can be written as $\boldsymbol{\sigma_A} = \sum_{i=1}^{n} \boldsymbol{\sigma_A^i}$, where n represents the totality of intervals of the potential with potential range $\boldsymbol{R} = \sum_{i=1}^{n} \boldsymbol{\delta_r^i}$. The absorption cross-section can be explicitly obtained at various intervals of the potential by using above expression. The fusion being an interior phenomena is expected to occur in the interior to the radial position of electrostatic Coulomb barrier, and the absorption in the region $0<r<R_B$ must account for the $\boldsymbol{\sigma_{fus}^{exp}}$ data. The exact radius R_{fus} up-to which absorption cross section is calculated for explaining $\boldsymbol{\sigma_{fus}^{exp}}$ is said to be fusion radius. Udagawa et al. [14,15] in their direct reaction model (DRM) use such concept of fusion cross-section. But they have considered fusion radius greater than RB in many heavy ion collisions analyzed, which allows fusion activity to start before reaching the Coulomb barrier RB. But fusion is normally assumed to happen after full penetration of barrier. Thus the concept will move opposite to the

common notion [16,17]. Therefore, this was severely criticized [18,19].

We overcome the above anomaly in our present discussion and consider the systems $^{12}C+^{208}Pb$, $^{16}O+^{208}Pb$,$^{19}F+^{208}Pb$, $^{16}O+^{144}Sm$, and $^{16}O+^{62}Ni$ in order to explain the experimental results of σ^{expt} by keeping R_{fus} smaller with respect to R_B. Without employing any numerical integration method including Runge-Kutta, we use an alternative approach for solving Schrödinger equation for given nucleus-nucleus potentials. Our approach is suitable for investigation of interval-wise absorption in the reaction process. The potential is simulated in our computation using arbitrarily tiny rectangular pieces. We establish an analytical formula for the scattering S-matrix in order to explain data, by employing accurate wave functions and their analytical continuation between neighbouring parts. The absorption level in each tiny portion or width of the potential is determined by using the same wave functions. As a result of which the overall reaction cross-section σ_r becomes the sum of contributions due to absorption across the whole range of potential. In contrast, we consider the total contribution for absorption across a constrained region $0 < r < R_{fus}$ inside R_B of the Coulomb barrier in order to explain why the fusion cross section σ_{fus} magnitude remains below σ_r. Interestingly, the outcomes obtained by using our approach well match results obtained from the method of Runge-Kutta.

In heavy nuclei collisions near the Coulomb barrier, measurements with excellent accuracy reveal data of σ_{fus} at relatively close energy intervals. For such a pair of heavy nuclei, the variation in the outcomes of $\sigma_{fus}$with the bombarding energy $E_{c.m.}$ in c.m. systemshows smooth fluctuation without any distinct characteristic, but it oscillates when light pairs of nuclei collide. It the product $E_{c.m.}\sigma_{fus}$ is doubly differentiated w.r.t. $E_{c.m}$ using some point difference formula, then function $D(E_{c.m.}) = \frac{d^2\,(E_{c.m.}\sigma_{fus})}{\mathrm{dE}^2_{\mathrm{c.m.}}}$ shows unusual oscillatory structure as energy $E_{c.m.}$varies [5]. This is referred to as barrier distribution. The experimental results of $D(E_{c.m})$ for the above cases are successfully explained in addressing peaks. The values of σ_{fus} obtained theoretically by using our method are presented in $D(E_{c.m.})$ form. In this study, we identify the following crucial traits in the potential that we used; in addition to being very deep and having little diffuseness, the real part is also highly strong compared to the imaginary part. Shape resonance states (experimentally not seen) [13] might endure throughout the collision process as a result of the formation of standing waves in the nuclear well because of the potential's less absorptive character. The oscillating structure in the results of $D(E_{c.m.})$ as a function of $E_{c.m.}$is consequently attributed to these resonances.

It should be noted that coupled-channels (CC) formulation is the natural language for investigating fusion processes at energies around the Coulomb barrier. For this, a number of computer programs, including CCFUS [20,21] and CCFULL[22], have been created. Since there are many channels present in the heavy ion collision process due to its complexity, solving coupled equations that take all of these channels into account is both difficult and time-consuming. These are nearly schematic formulations. This method includes key approximations in order to simplify the calculation process. In the majority of pairings of nuclei, the aspects of both σ_{fus} and $D(E_{c.m.})$ cannot be explained satisfactorily even with exhaustive CC calculation. This unsatisfactory circumstance is still present in the most current CC projections [23] based on M3Y plus repulsion potential used for analyzing data of the $^{16}O+^{208}Pb$ system.

According to a most recent calculation [24], even observed value of σ_{fus} from the sub-barrier region through above barrier region cannot be concurrently estimated by CC calculations with identical the nuclear potential of Woods-Saxon. The CC calculation in microscopic level is essentially one dimensional model of crossing the barrier [25,26] that includes lots of barriers with different heights that are produced as a result of coupling between the relative motion and the internal degrees of freedom of the colliding nuclei, such as static deformation, collective vibration [27], inelastic excitation, and nucleon transfer [23]. For imposing boundary condition for the barrier crossing model, the coupled-channel calculation for cross section of fusion scarcely takes the impact of any mechanism of the interaction potential in the interior pocket into account because it is believed to be exceedingly absorptive.

The potential considered for nucleus-nucleus interaction in pocket area is a key component of the current formulation and is used to explain the experimental results of σ_{fus} as well as the related function $D(E_{c.m.})$ generated from measured σ_{fus}. Due to the pocket's less absorptive character, the resonances that it produces successfully depict the oscillatory structure of $D(E_{c.m.})$. Further more, although it is not stated directly in our model, the impact of coupling is implied. It is anticipated that the entrance channel potential barrier would vary dramatically when a non-elastic channel is coupled with it [28], especially in region $r < R_B$, where the effective potential will suddenly drop [29,30]. By choosing small diffuseness parameter in the Woods-Saxon potential, this coupling effect may be easily included in the formulation. The current formulation includes the influence of coupling of channel in a phenomenological fashion by using such a modest diffuseness value in the analysis of scattering cross-sections and fusion cross-sections simultaneously. We discuss in section 1.2 the formulation regarding analytical expression for the S-matrix and region-wise absorption. We apply our theory in section 1.3 to explain bserved data of $\frac{d\sigma(\theta)}{d\sigma_R(\theta)}$, $\sigma_{fus}(E_{c.m.})$ and $D(E_{c.m.})$ for the systems $^{12}C+^{208}Pb$, $^{16}O+^{208}Pb$, $^{19}F+^{208}Pb$, $^{16}O+^{144}Sm$, and $^{16}O+^{62}Ni$. The various results of discussions are summarized in section 1.4.

II. FORMULATION

Nuclear optical model is frequently employed to study collisions of heavy ions. The most important component of scattering and reaction cross-sections is to solve the radial Schro¨dinger equation by using a complex potential. The potential has different parts. The complex nuclear potential $V_N(r)$, Coulomb potential $V_C(r)$, and the centrifugal component $V_\ell(r)$ are added to provide the necessary effective potential to solve radial equation. While solving the Schro¨dinger equation for this potential, people usually follow the Runge-Kutta method (RK) of numerical integration to get wave function. The derivative of the wave function is also obtained outside the nuclear potential range. This wave function and derivative are further utilized to Coulomb wave function and the derivative of the function to get the results of scattering matrix with an aim to analyse experimental data. However, with this procedure, it is not simple to separate a portion of reaction cross-section from the whole cross-section in order to explain fusion cross-section. As a result, we use a practical but slightly different method to resolve the Schro¨dinger equation [31–33].

Let's start by carefully examining the S-wave dispersion. A chain of 'n' rectangular potentials, each with an arbitrarily small width 'w', can be thought of as a potential U(r). In reality, a similar method is implied in any numerical integration of a differential equation. After simulating the potential up to the r = R_{max}, we have $R_{max} = \sum_i^n w_i$, where $w_i = w$ is the width of the ith rectangle. Let in the jth region, $\sum_{i=1}^{j-1} w_i < r \leq \sum_{i=1}^{j} w_i$, the strength and width of the potential are denoted by U_j and w_j respectively.

The reduced Schrödinger equation in this region is given as

$$\frac{d^2\phi(r)}{dr^2} + \frac{2m}{\hbar^2}\left(E - U_j\right)\phi(r) = 0 \tag{1}$$

with the solution given as

$$\phi_j(r) = a_j e^{ik_j r} + b_j e^{-ik_j r} \tag{2}$$

where the wave number k_j is defined as $k_j = \sqrt{\frac{2m}{\hbar^2}(E - U_j)}$ for j^{th} segment having width w_j. For both the adjacent segments, we use notation $q_{ji} = -q_{ij} = \frac{k_j - k_i}{k_j + k_i}$. Here, m denotes the particle's mass and E denotes the incident energy. The solution may be expressed in the first three segments near the origin and r = 0 as

$$\phi_I = \sin k_1(r - c_1), 0 < r < w_1, w_1 < r < (w_1 + w_2) \tag{3}$$

$$\phi_{II} = a_2 e^{ik_2(r-c_2)} + b_2 e^{-ik_2(r-c_2)}, \quad w_1 < r < (w_1 + w_2) \tag{4}$$

$$\phi_{III} = a_3 e^{ik_3(r-c_3)} + b_3 e^{-ik_3(r-c_3)}, \quad (w_1 + w_2) < r < (w_1 + w_2 + w_3) \tag{5}$$

Here $a_2,\ b_2,\ a_3,\ and\ b_3$ are coefficients of the wave functions and $c_1, c_2\ and\ c_3$ are arbitrary constants.

When the wave functions is matched with its derivatives near boundary at $r = w_1$, we have

$$a_2 = \frac{1}{2} e^{-ik_2(w_1 - c_2)} \left[\sin k_1(w_1 - c_1) + \frac{k_1}{ik_2}\cos k_1(w_1 - c_1)\right] \tag{6}$$

$$b_2 = \frac{1}{2} e^{ik_2(w_1 - c_2)} \left[\sin k_1(w_1 - c_1) - \frac{k_1}{ik_2}\cos k_1(w_1 - c_1)\right] \tag{7}$$

$$\frac{a_2}{b_2} = e^{-2ik_2(w_1 - c_2)} \times q_{21} \tag{8}$$

Where,

$$q_{21} = \frac{\sin k_1(w_1 - c_1) + \frac{k_1}{ik_2}\cos k_1(w_1 - c_1)}{\sin k_1(w_1 - c_1) - \frac{k_1}{ik_2}\cos k_1(w_1 - c_1)} \tag{9}$$

Similar calculation at the boundary at $r = (w_1 + w_2)$ yields

$$a_3 = \frac{1}{2} e^{-ik_3(w_1+w_2-c_3)} b_2 e^{-ik_2(w_1+w_2-c_3)} \times \left[\left(1-\frac{k_2}{k_3}\right)+\left(1+\frac{k_2}{k_3}\right)e^{2ik_2w_2}q_{21}\right] \tag{10}$$

$$b_3 = \frac{1}{2} e^{ik_3(w_1+w_2-c_3)} b_2 e^{-ik_2(w_1+w_2-c_3)} \times \left[\left(1+\frac{k_2}{k_3}\right)+\left(1-\frac{k_2}{k_3}\right)e^{2ik_2w_2}q_{21}\right] \tag{11}$$

$$\frac{a_3}{b_3} = e^{-2ik_3(w_1+w_2-c_3)} \times q_{321} \tag{12}$$

Where, (13)

$$q_{321} = \frac{q_{32}+q_{21}e^{2ik_2w_2}}{1+q_{32}\times e^{2ik_2w_2}}$$

and (14)

$$q_{32} = \frac{k_3-k_2}{k_3+k_2}$$

This can be generalized for n boundaries to give

(15)

$$\frac{a_n}{b_n} = e^{-2ik_n\left(\sum_{j=1}^{n-1} w_j - c_n\right)} \times q_{n,n-1,n-2,\ldots\ldots\ldots\ 1}$$

(16)

$$q_{n,n-1,n-2,\ldots\ldots\ldots\ 1} = \frac{q_{n,n-1}+q_{n,n-1,n-2,\ldots\ldots\ldots\ 1}e^{2ik_{n-1}w_{n-1}}}{1+q_{n,n-1}\times q_{n,n-1,n-2,\ldots\ldots\ldots\ 1}e^{2ik_{n-1}w_{n-1}}}$$

$$\vdots$$

(17)

$$q_{21} = \frac{\sin k_1(w_1-c_1)+\frac{k_1}{ik_2}\cos k_1(w_1-c_1)}{\sin k_1(w_1-c_1)-\frac{k_1}{ik_2}\cos k_1(w_1-c_1)}$$

Where,

$$q_{n,n-1} = \frac{k_n-k_{n-1}}{k_n+k_{n-1}}$$

Setting the arbitrary constants as $c_1 = w_1$ and $c_n = \sum_{j=1}^{n-1} w_j$
We get,

$$D^{(0)} = \frac{a_n}{b_n} = q_{n,n-1,n-2,\ldots\ldots\ldots\ 1} = \frac{q_{n,n-1}+q_{n,n-1,n-2,\ldots\ldots\ldots\ 1}e^{2ik_{n-1}w_{n-1}}}{1+q_{n,n-1}\times q_{n,n-1,n-2,\ldots\ldots\ldots\ 1}e^{2ik_{n-1}w_{n-1}}} \tag{18}$$

With, (19)

$$q_{\ n-1,n-2,\ldots\ldots\ldots\ 1} = \frac{q_{n-1,n-2}+q_{\ n-2,n-3,\ldots\ldots\ldots\ 1}e^{2ik_{n-2}w_{n-2}}}{1+q_{n-1,n-2}\times q_{n-2,n-3,\ldots\ldots\ldots\ 1}e^{2ik_{n-2}w_{n-2}}}$$

$$\vdots$$

$$q_{21} = -1 \tag{20}$$

The function in m-region may be defined in terms of that in the (m-1) area using their cursive nature of the formula for $q_{n,n-1,n-2,\ldots\ldots\ldots\ 1}$. This allows us to simulate the potential given by U(r) by n-step potentials and further create an easy-to-use numerical program for assessment of scattering S-matrix and also the wave function at certain energy. We assume $\sum_{i=1}^{n} w_i = R_n = R_{max}$, such that the potential $U_j(r))$ is zero for $r > R_n$ [Eq.1]. Now it is simple to say that the S-wave S-matrix is given by $s_0 = -\frac{a_n}{b_n}$. Total absorption (reaction) cross-section in region $0 < r < R_n$ is given by

$$\sigma_{abs}^{(0)} = \frac{\pi}{k^2}\left(1 - \frac{|a_n|^2}{|b_n|^2}\right)$$

Similarly, $S_0^p = -\frac{a_p}{b_p}$ is taken as S-matrix of the original potential which is trimmed at $R_p(=\sum_{i=1}^{p} w_i) < R_{max}$. Hence $\frac{\pi}{k^2}\left(1 - \frac{|a_p|^2}{|b_p|^2}\right)$ can be taken as the absorption cross section generated in the region $0 < r < R_p$. Thus $\frac{\pi}{k^2}\left[\left(1 - \frac{|a_p|^2}{|b_p|^2}\right) - \left(1 - \frac{|a_q|^2}{|b_q|^2}\right)\right]$ shall give the contribution to the absorption cross section from the region$R_p > r > R_q = \sum_{i=1}^{q} w_i$.

We obtain complex conjugate of eq.(1) and rearrange to get

$$2ik_n(|a_n|^2 - |b_n|^2) = \int_0^{R_n} 2iImU(r)\phi\phi^* dr \tag{21}$$

$$1 - \frac{|a_n|^2}{|b_n|^2} = I_1 + I_2 + \cdots \tag{22}$$

$$I_1 = -\frac{1}{k_n}\int_0^{w_1} ImU(r)\left|\frac{\phi}{b_n}\right|^2 dr \tag{23}$$

$$I_2 = -\frac{1}{k_n}\int_{w_1}^{w_1+w_2} ImU(r)\left|\frac{\phi}{b_n}\right|^2 dr \tag{24}$$

We simplify the associated integral using the appropriate wave function and the potential in a specific section and obtain

$$1 - \frac{|a_n|^2}{|b_n|^2} = \sum_{j=1}^{n} I_j \tag{25}$$

With,

$$R_n = \sum_{j=1}^{n} w_j = R_{max} \tag{26}$$

Considering same width for all segments, i.e $w = w_1 = w_2 = w_3 = \ldots$, we have $n = \frac{R_{max}}{w}$.

$$I_j = \left(-\frac{1}{k_n}\right)\frac{ImU_j}{|b_n|^2}\left\{\frac{|b_j|^2}{2Imk_j}e^{-2Imk_j w_{j-1}}\left(e^{2Imk_j w_j}-1\right)\right.$$
$$-\frac{|b_j|^2}{2Imk_j}e^{2Imk_j w_{j-1}}\left(e^{-2Imk_j w_j}-1\right) \quad (27)$$
$$\left.+\frac{1}{Rek_j}Im\left[a_j b_j^* e^{2Imk_j w_{j-1}}\left(e^{2iRek_j w_j}-1\right)\right]\right\}$$

The complex conjugate is represented by an asterisk mark. S-matrix calculation procedure through equations (18), (19) and (20) with a *multistep potential* (MP), an algebraic recursive technique is used for approximation.. This can be programmed easily. The equations (27), (28) and (29) provide a method for study of absorption cross section as the discrete sums of different contributions from different sections.

It is simple to generalize this method to the challenging heavy ion Coulomb nuclear issue for any partial wave. One may use the MP approximation approach for this effective potential to handle higher partial wave problems as the scattering by $V_N(r)+V_C(r)+V_\ell(r)$. The complexity of the $r^{\ell+1}$ behaviour of the wave function close to origin in the complex potential scattering is not particularly important for the following reasons. The properly normalized wave function typically attenuates quickly to zero well beyond the origin for absorptive complex potential due to the existence of absorption. As a result, one may begin the S-matrix computation well after r = 0, in which region multistep approximation is more precise. We have confirmed that the cross-section and S-matrix findings produced by our strategy are nearly identical to those produced by traditional methods.

The effective potential has three parts, i.e., $V_N(r)$, $V_C(r)$ and $V_l(r)$ in $0 < r \leq R_{max}$. But the potential is merely Coulombic $[V_C(r)]$ in the outer region, i.e., in $r \geq R_{max}$. The last term $V_l(r = \frac{\hbar^2}{2m}\frac{l(l+1)}{r^2}$ is centrifugal term for different momentum partial wave l.

By using the exact Coulomb wave functions i.e $G_l \; and \; F_l$ and their derivatives $G_l^{'} \; and \; F_l^{'}$, in the outer region $r \geq R_{max}$ and the wave function $\phi_n(r) = a_n e^{ik_n r} + b_n e^{-ik_n r}$ and its derivative $\phi_n^{'}(r)$ in the left side of r= R_{max} , we get the expression for partial wave S-matrix η_l as

$$\eta_l = 2iC_l + 1 \quad (28)$$

Where,
$$C_l = \frac{KF_l' - F_l H}{H(G_l + iF_l) - K(G_l' + iF_l')} \quad (29)$$

$$H = \frac{\phi_n'}{\phi_n} = ik_n\frac{D^{(l)}e^{ik_n R_{max}} - e^{-ik_n R_{max}}}{D^{(l)}e^{ik_n R_{max}} + e^{-ik_n R_{max}}} \quad (30)$$

$$D^{(l)} = \frac{a_n}{b_n} \quad (31)$$

With, $K_n = \sqrt{\frac{2m}{\hbar^2}(E - V_n)}$, which is real at $r = R_{max}$,, where the potential $V_n = V_C + V_l$ is real and $E > V_n$

We describe the elastic scattering of a particular system using the preceding formula (30)

for□□. The formula may be used to calculate the reaction cross-section.

(32)

$$\sigma_r = \frac{\pi}{K^2}\sum_l (2l+1)(1-|\eta_l|^2)$$

As formulated above this is equal to the absorption cross section

$$\sigma_{abs} = \sum_l (2l+1)\left(1 - \frac{|a_n|^2}{|b_n|^2}\right) = \frac{\pi}{k^2}\sum_l (2l+1)\left[\sum_{j=1}^{n} I_j^{(l)}\right] \quad (33)$$

By taking into account the matching number of segments in the aforementioned summation, it is possible to determine the contribution of any component with in the range $0R_{max}$ to the absorption or reaction cross section. With no potential disturbance, this analysis of the collision process's region-by-region absorption results in the wave function that characterises the angular distribution of the elastic scattering data. If someone wants to know how much absorption cross section is there in the region $0 < r < R_{fus}$, where$R_{fus} < R_{max}$, the total number of segments to be considered in the summation (35) is $n_{fus} = \frac{R_{fus}}{w}$. The resulting cross section in given below in Eq.(34). This cross-section refers to fusion in the context of DRM [14] mentioned earlier.

$$\sigma_{fus} = \frac{\pi}{k^2}\sum_l 2l+1)\left[\sum_{j=1}^{n_{fus}} I_j^{(l)}\right] \quad (34)$$

It might be beneficial at this point to briefly explore MP formulation as a numerical approach. In comparison to the trapezoidal rule, Simpson's rule and spline technique (by using straight-line sections, parabolic sections and cubic polynomials respectively), this method, in a sense, is the most simple approximation to solve differential equations [34–36].The latter techniques are highly helpful for computing the wave function with more accuracy, but they have the drawback of being difficult to describe algebraically in terms of simple intervals. The computation upto 3-4 significant places after decimal point of wave function and the cross-section, however, is fairly suitable to calculate cross-section given the experimental uncertainties involved. In a study [37], we compared the numerical results for potentials like Eckart and Ginocchio potentials produced using the MP technique in one dimension with those obtained using the R-K and exact solution, and we discovered that the results agreed upto three significant places. This section has demonstrated how the analytical formulation results in a tidy recursive relation that makes it easier to calculate cross-sections

and S-matrices. With this MP formulation, it is possible to transparently estimate the contribution to absorption in various potential segments and examine the wave function nature and the normalization. However, the wave function rises quickly in the calculations for the nucleus-nucleus optical model performed using the R-K method [38] due to the imaginary potential and should be renormalized at various stages in order to perform calculations of effective phase-shift. This makes it more difficult to estimate the regional contributions to the reactions and the cross-sections [39]. To demonstrate the effectiveness and usefulness of our MP technique, we compute elastic scattering cross-sections and fusion cross-sections in HICs (heavy-ion collisions) and satisfactorily explain the experimental outcomes. The numerical outcomes of the elastic scattering cross sections provided in Ref [38] are validated using conventional optical model techniques.

Table 1: Optical Model Potential Parameters Used in the Calculations.
(V^B represents height and R^B radial position of the Coulomb barrier)

System	V_N (MeV)	r_V (fm)	a_V (fm)	W (MeV)	r_W (fm)	a_W (fm)	r_C (fm)	V_B (MeV)	R_B (fm)	R_{fus} (fm)
$^{12}C+^{208}Pb$	125	1.31	0.320	3.0	1.325	0.25	0.90	56.7	12.16	9.9
$^{16}O+^{208}Pb$	125	1.35	0.285	2.0	1.320	0.15	1.02	73.7	12.52	8.8
$^{19}F+^{208}Pb$	105	1.35	0.285	2.0	1.320	0.15	1.37	81.51	12.74	8.3
$^{16}O+^{144}Sm$	100	1.295	0.365	4.0	1.250	0.15	1.1	60.25	11.46	10.0
$^{16}O+^{62}Ni$	75	1.333	0.380	6.0	1.250	0.33	1.04	30.41	10.2	7.78

III. APPLICATION

The formulation which is developed in section 1.2 is applied for data analysis of the systems $^{12}C+^{208}Pb$, $^{16}O+^{208}Pb$, $^{19}F+^{208}Pb$, $^{16}O+^{144}Sm$ and $^{16}O+^{62}Ni$. We obtain a reliable explanation of the experimental cross-section magnitudes regarding fusion and elastic scattering. We also find interesting peaks in variation of $D(E_{c.m}) = \frac{d^2(E_{c.m}.\sigma_{fus})}{dE_{c.m}^2}$ against the energy $E_{c.m.}$.

The optical model potential (OMP) in the entrance channel is described by

$$V(r) = -V_N f(r, R_v, a_v) - i\,W g(r, R_w, a_w) + V_c(r)$$

Here, the analysis involves two nuclei with mass number A_1 and A_2. Their proton numbers are Z_1 and Z_2 respectively. We use the form factor in this paper as described below

$$f(r,R,a) = g(r,R,a) = \left[1 + exp\left\{{}^{(r-R)}/_{a}\right\}\right]^{-1}$$

The symbol V_N represents the real part of OMP, whereas, W represents the strength of

imaginary part. Radius parameters are given as $r_V = \frac{R_V}{\left(A_1^{\frac{1}{3}}+A_2^{\frac{1}{3}}\right)}$ and $r_W = \frac{R_W}{\left(A_1^{\frac{1}{3}}+A_2^{\frac{1}{3}}\right)}$. The symbols a_V and a_W are the diffuseness parameters. The Coulomb potential $V_C(r)$ is given by

$$V_c(r) = \frac{z_1 z_2 e^2 \left(3 - {r^2}/{R_c^2}\right)}{2R_c} \qquad r \le R_c\,;$$
$$V_c(r) = {z_1 z_2 e^2}/{r} \qquad r > R_c\,,$$

Where, $R_c = r_c(A_1^{\frac{1}{3}} + A_2^{\frac{1}{3}})$ with r_C as the Coulomb radius parameter. Thus there are a total of seven parameters, namely, V_N, r_V, a_V, W, r_W, a_W and r_C in this potential.

1. **Elastic scattering cross-section:** The angular distribution of elastic scattering can be explained by a number of different sets of potential-descriptive parameters, according to what we know. All seven parameters in our current calculation are independent of energy. While choosing parameter values, we keep the fact in mind that resonance occurs when the imaginary part is kept low. The weak absorption is appreciable when real part is assumed to be deep [40] and also less diffused [41] to account for the cross-sections of elastic scattering. The parameter values used for analysis of systems ^{12}C+^{208}Pb, ^{16}O+^{208}Pb, ^{19}F+^{208}Pb, ^{16}O+^{144}Sm , and ^{16}O+^{62}Ni are given in Table 1.1 along with height (V_B) and radius (R_B) of S-wave barrier in case of each collision system.

   - **^{12}C+^{208}Pb system:** According to the prescription mentioned above, the real portion in case of ^{12}C+^{208}Pb is made more deep with a depth of V_N = 125 MeV. It is also taken less diffused with a diffuseness parameter of a_V = 0.32 fm and a radius parameter of r_V = 1.31 fermi. Again, the corresponding imaginary component also receives the additional parameters r_W = 1.325 fm, a_W = 0.25 fm and W = 3.0 MeV. The attractive strength is taken small. The Coulomb radius parameter assumes a value of r_C = 0.9 fm. Real part of the combined nuclear and Coulomb potentials for an s-wave is shown in **Fig.1** as a function of radial distance for visual illustration. This demonstrates the repulsive barrier for the ^{12}C+^{208}Pb system with height V_B= 56.7 MeV and position R_B = 12.16 fm lowering quickly in the inner side. According to the formulation, 'n' rectangular potentials, each with a width of 0.008 fm, are used to replicate the potential in the area $0 < r \le R_{max}$. The nuclear potential together with its imaginary portion is zero in the area $r > R_{max} \approx 15$ fm, leaving the effective potential as the sum of Coulombic and centrifugal term.

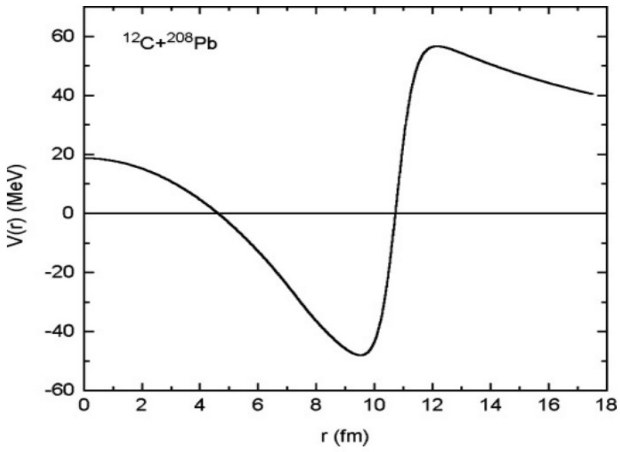

Figure1: Plot of the real part of nuclear plus Coulomb potentials against radial distance with l=0 and with potential parameters V_0= –125MeV, r_V = 1.31fm, a_V = 0.32fm, and r_C = 0.9 fm for the $^{12}C+^{208}Pb$ system.

Using the S-matrix given by the expression (1.28), at laboratory energies of 58.9, 60.9, 62.9, 64.9, 74.9, and 84.9 MeV, we get the findings of angular change of differential scattering cross-section. These computed findings are displayed as solid curves in Fig.2. They are contrasted with the comparable experimental data from Ref.[1]. The experimental data are depicted in the same figure as solid circles.

It is obvious that the data explanation in each energy case is fairly sound. It should be noted that we utilized exactly the same set of OMP values listed in Table 1.1 to explain the results for energies between 58.9 MeV and 84.9 MeV. In other words, OMP parameter values are independent of energy. We should also point out that the value of r_C=0.9fm that we are considering is a little lower than the standard value of r_C = 1.25 fm. This fact is supported by the calculation's conclusion in Ref. [42] about Coulomb potentials in HICs, which shows that it has no impact on the outcomes of the elastic collision (cross-section) in our calculation. This lower value of r_C has been utilized to consistently explain fusion cross-section for the $^{12}C+^{208}Pb$ system at the low energy. This will be covered in the next section.

- **$^{16O}+^{208}$Pbsystem:** We have taken into consideration a deep real potential in this instance as well, with depth V_N = 125 MeV. The value of diffuseness parameter taken small, i.e., a_V = 0.285 fm. Other parameters have been given in Table 1.1. The barrier lowering steeply in the inner side with a height of V^B = 73.7 MeV and a radius of R_B=12.52 fm for this system can be seen in the graph of real component of nuclear plus Coulomb potentials against radial distance for s-wave in Fig.3.

Figure 4 shows a comparison between our projected differential scattering cross-section values (solid curves) and the corresponding experimental values (shown with solid circles) from Reference [2] at various laboratory energies, including 80, 83, 88, 90, 96 and ^{102}MeV. It is obvious that the data's explanation for all energies is sound. Additionally, a single potential is employed for all energies in this case, but with low value of r_C = 1.02fm.

- **^{19}F+^{208}Pb system:** The potential depth is taken to be V_N = 105 MeV and the diffuseness parameter is taken to be A_V = 0.285 fm for the system ^{19}F+^{208}Pb. The depth is taken high, whereas, diffuseness parameter is taken small. Other parameters are mentioned in Table 1.1 with a set of values suitable for analysis. Using the S-matrix given by equation (1.28), the results of angular variation of differential scattering cross-section at energies 88.0, 91.0, 93.0, 96.0, 98.0 and 102.0 MeV in laboratory frame are calculated. In Fig.5,these computed results are depicted as solid curves, and they are compared with the experimental data from Ref.[6], which are displayed as solid circles in the same figure. It is obvious that the data's explanation for all energies is reasonable.

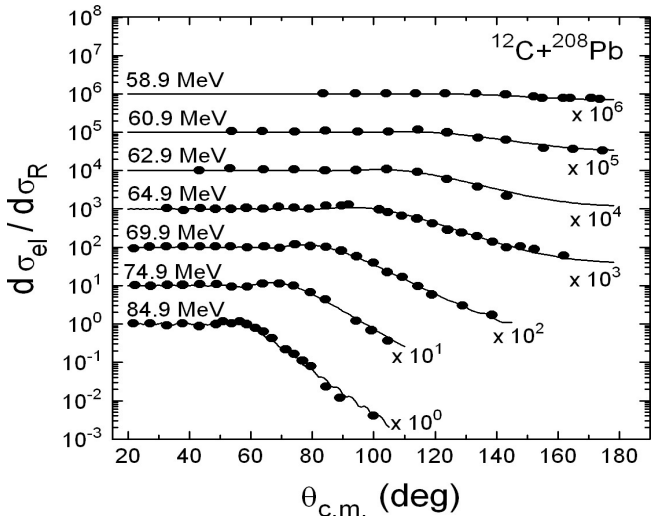

Figure 2: Plotting of scattering cross sections with respect to Rutherford's cross section for elastic collision system ^{12}C+^{208}Pb. Energies are mentioned in laboratory frame. The angular distribution is given as a function of $\theta c.m.$. Theoretical calculations are given by solid curves. Solid circles represent experimental data taken from Ref.[1].

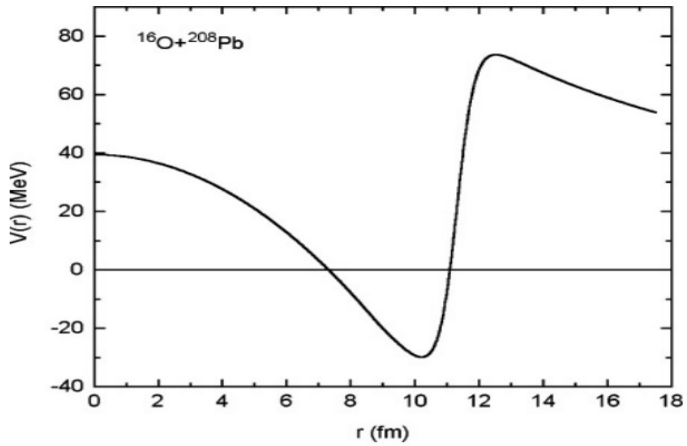

Figure3: Plotting of real part of effective potential (nuclear plus Coulomb potential) against radial distance for l=0 and with parameters, V_0= -125MeV, r_V=1.339fm, a_V=0.285fm, and r_C=1.02 fm for $^{16O+208}$Pb system.

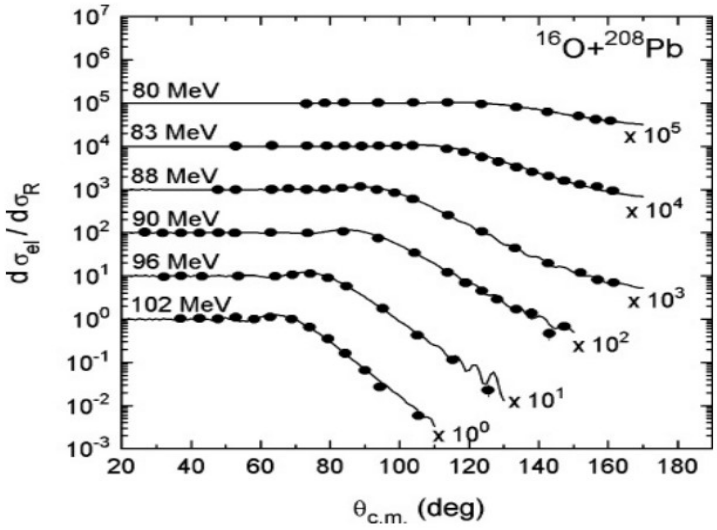

Figure 4: Same as Fig. 2 for system $^{16}O+^{208}Pb$ at 80, 83, 88, 90, 96, and 102 MeV energies in laboratory frame. The solid curves represent theoretical results and solid circles represent experimental data taken from Ref.[2].

- **$^{16}O+^{144}$ Smsystem:** Similar calculations are done for this system. A deep real potential has been chosen with VN = 100.0 MeV and a minimal diffuseness value of a^V = 0.365 fm in this case as well. Values of other parameter are given in Table 1.1. The plotting in Figure-6 compares the calculated values of differential scattering cross-section (solid curves) with experimental data (solid circles) from Ref.[8] at various energies, i.e., 66.0, 69.2 and 72.3 MeV. It is seen that the agreement of our theoretical results with experimental data is quite good.

- **16O+62 $_{Nisystem}$:** Here, we have used the optical potential parameters of 16O+58_{Ni} system except r^V = 1.333 fm. In Fig. 7, we compare the differential cross-sections computed theoretically for scattering (given as solid curves) with corresponding experimental data (given as solid circles) obtained from references [11] at various energies, i.e., 42.0, 48.0 and 54.0 MeV. It is clear from the graphs that the above experimental data are successfully reproduced by our method simultaneously.

Now it is essential to use the same potential in the description of fusion data. The analyses are carried out below for the afore-mentioned systems. The finding of an optical model potential (OMP) which is energy independent is a significant conclusion of our research and discussion.

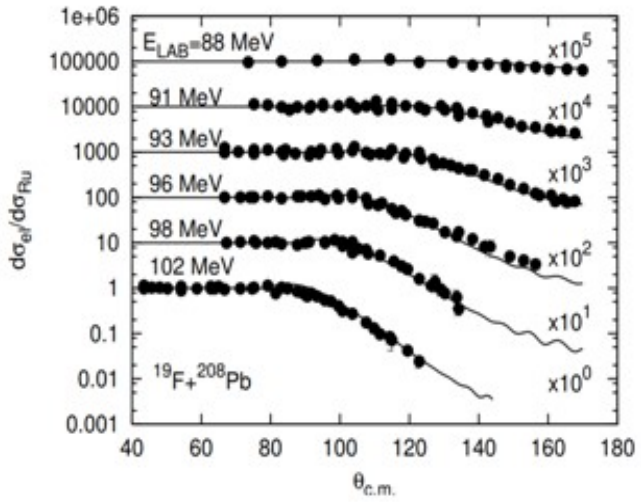

Figure 5: Angular distribution of elastic scattering cross sections (ratios to Rutherford) as a function of $\theta c.m.$ of $^{19}F+^{208}Pb$ system at different laboratory energies. The full drawn curves are theoretical results of our optical model calculation. The solid circles are experimental data taken from Ref.[6].

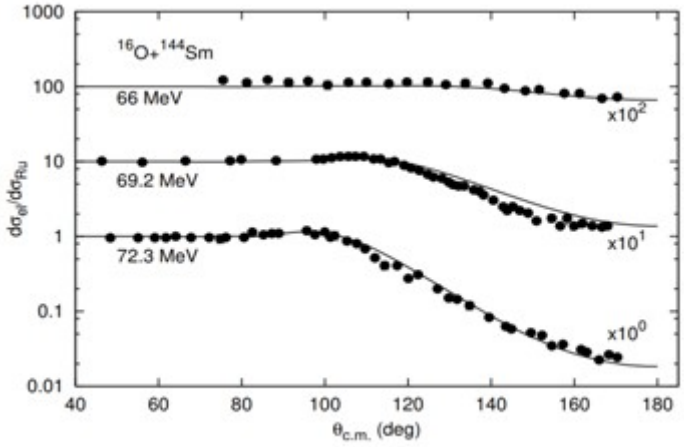

Figure 6: Angular distribution of elastic scattering cross sections (ratios to Rutherford) as a function of $\theta c.m.$ of $^{16}O+^{144}Sm$ system at differentlaboratory energies. The full drawn curves are theoretical results of our optical model calculation. The solid circles are the experimental data taken from Ref.[8].

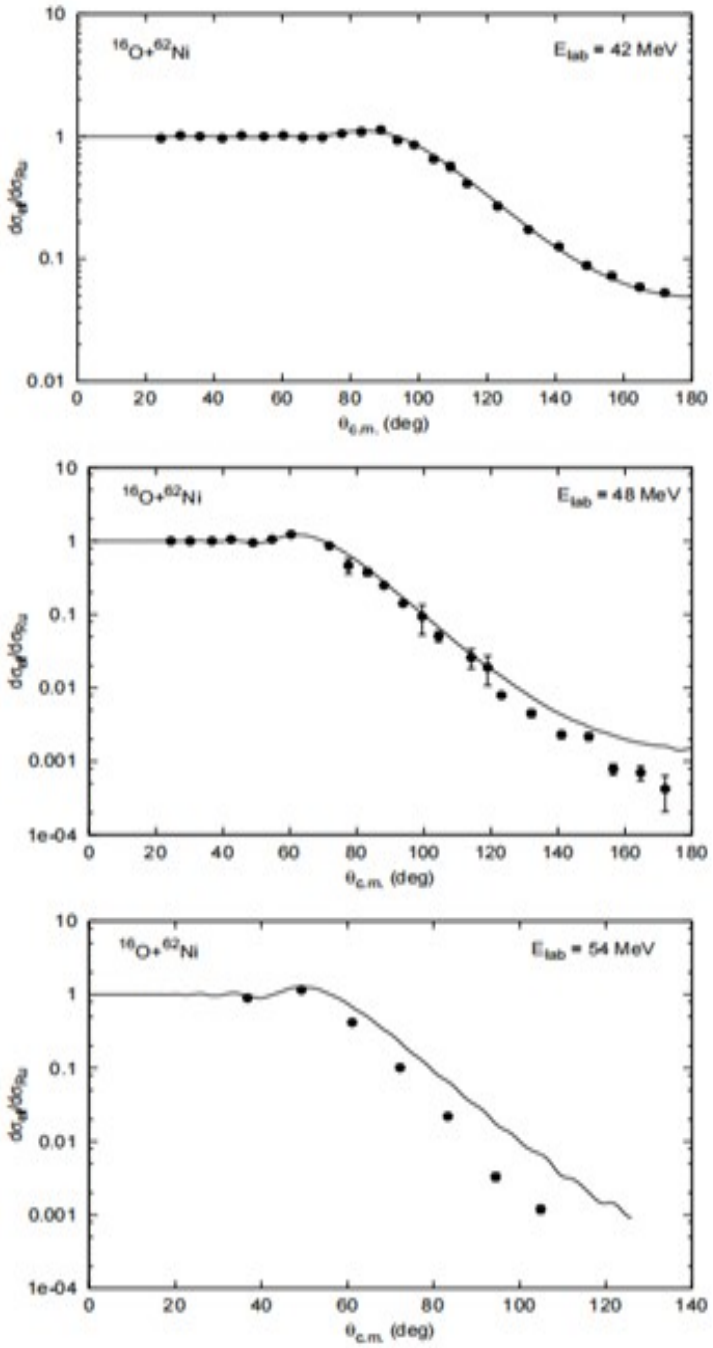

Figure 7: Angular distribution of elastic scattering cross sections (ratios to Rutherford) as a function of $\theta_{c.m.}$of $^{16}O+^{62}Ni$ system at differentlaboratory energies. The full drawn curves are theoretical results of our optical model calculation. The solid circles are experimental data taken from Ref.[11].

2. **Fusion cross-section:** Fusion of the two nuclei is a crucial mechanism. It is actively linked to the elastic collision process in low energy range. It is simple to take into account that cross-section, σfus, of fusion is a portion of the overall reaction cross section σ_r, when estimating total cross-sections of scattering as well as fusion. However, it is never

easy to take a part from σr that precisely accounts for the observed results of fusion at different incidence energy across a large range. In order to compute σfus, we take into account the DRM of Udagawa et al. [14]. The quantity of absorption cross-section inside the inner zone $0 < r < R_{fus}$ is what this model refers to as the fusion cross-section. Here Rfus is radial distance which is expected to be smaller than R^B. R^B is the radial position of S-wave Coulomb barrier in case of a given nuclear system. Ee have calculated in Eq.(1.34) the cross-section values of σ_{fus} according to DRM principle.

- **^{12}C+^{208}Pb System:** We obtain the results of σ_{fus} for the system $^{12}C+^{208}Pb$ by using R_{fus}= 9.9 fm. In Fig.8, the theoretical results (solid curve) so obtained are compared with experimental results (solid circles) collected from Reference [3]. It is evident from the graphs that the data fairly match throughout the whole energy range, i.e., from $E_{c.m.}$= 50 MeV to 75 MeV. The OMP parameters, whose values explain scattering data in Fig.2, have not been altered in order to achieve this fitting. The values of R^{fus}= 9.9 fm utilized in our computation are smaller than Coulomb radius R^B=12.16 fm, which is required by the permissible state of reality. The present successful description of scattering and fusion cross-sections is more important because of the fact [3,26] that Woods-Saxon potential fails to explain.

- **^{16O}+^{208}Pb System:** Remarkable accomplishment is attained in case of 16O+208$_{Pb}$ system, where our calculated results (solid curve) are able to reproduce experimental results as indicated by solid dots of σfus taken from Reference [4] for the given range of energy from $E^{c.m}$.=68 MeV to $E^{c.m}$.= 86 MeV. Here, fusion radius, R^{fus}=8.8 fm is small compared to Coulomb radius R^B = 12.52 fermi. Unlike in case of 12C+208$_{Pb}$, inthis16O+208$_{Pb}$ system, we need slight modification of nuclear radius parameter r^V=1.35 fm (Table1.1). This is taken for analyzing scattering data and take r^V = 1.339 fm for the fitting of measured σ^{fus} data.

- **^{19F}+^{208}Pb system:** In this case, we have used the fusion radius R^{fus}=8.3 fm. This radius is smaller than the Coulomb radius, which is taken as R_B=12.74 fm. We compare, in Fig.10,our calculated cross-sections of fusion with the corresponding experimental cross-sections obtained from Ref. [7]. In order to get a good fitting in fusion cross section, we modify the nuclear radius parameter slightly from r_V = 1.35 fm to r^V = 1.356 fm for successful analysis of experimental elastic scattering results.

- **^{16O}+^{144}Sm system:** When our calculated results (solid curve) are compared with the experimental results shown by solid dots of cross-section σ_{fus} taken from Ref. [9] for the $^{16O}+^{144}$Sm system as shown in Fig.11,a similar result is achieved. The fusion radius in this instance, R_{fus}=10.0 fm, is less than the Coulomb radius, RB=11.46 fm. The nuclear radius parameter, r_V, which was previously set at 1.145 fm (Table 1.1) for the analysis of scattering data must now be changed to 1.295 fm for fair reproduction of observed σ_{fus} data.

- **^{16O}+^{62} Ni Collision System:** We have taken R_{fus}=7.78 fm which is less than R_B=10.20 fm. The calculated values (as shown by solid curve) of fusion cross-section is compared with the experimental results (given as solid circles) taken from Ref.[11]in Fig.12.It is clear from the figure that the theoretical results is in excellent agreement

with the experimental data. To achieve this we have slightly changed the r_V value from 1.333fm (used for elastic scattering calculation) to 1.313fm.

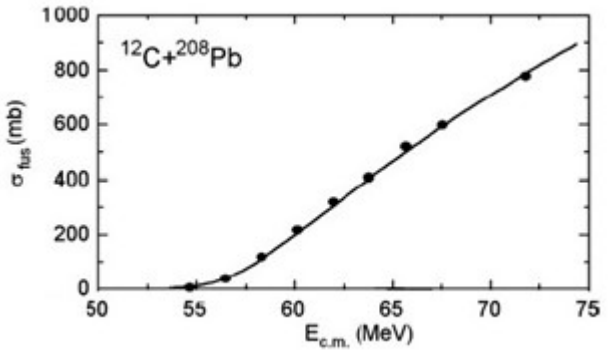

Figure 8: Variationof fusion cross section σ_{fus}as a functionof energy $E_{c.m.}$forthe $^{12}C+^{208}Pb$ system. The solid and continuous curve represents our theoretical calculation. Experimental data which are shown by solid circles are found from Ref.[3].

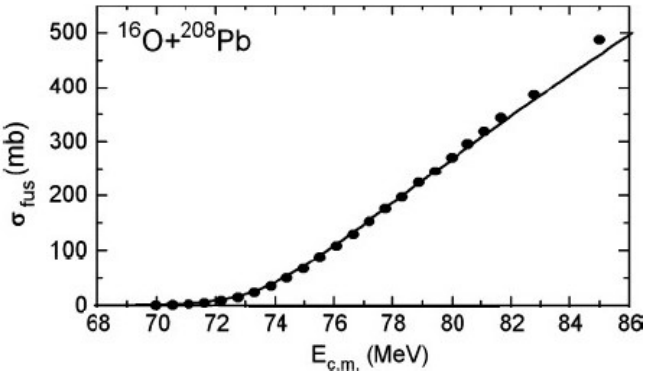

Figure 9: Variation of cross-section σ_{fus} as a function of $E_{c.m.}$ for the $^{16}O+^{208}Pb$ system. The solid curve represents our theoretical calculation. Experimental values which are shown by dark circles are found from Ref.[4].

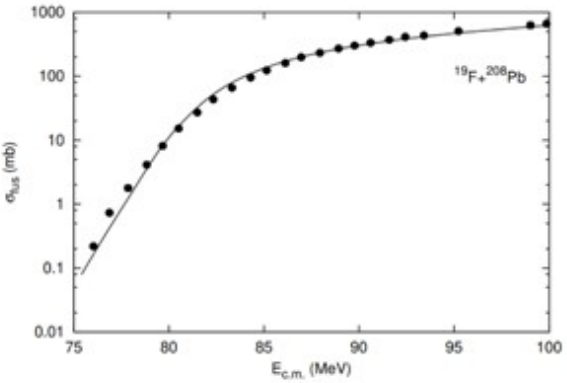

Figure 10: Variation of fusion cross-section σ_{fus} as a function of energy $E_{c.m.}$ for the $^{19}F+^{208}Pb$ system. The continuous curve represents our theoretical calculation. Experimental data are represented by dark circles. The experimental data are found from Reference [7].

The fusion radius R_{fus} values we utilized in our calculations are, however, smaller in all of these systems than the corresponding Coulomb radius R_B values. This indicates unequivocally that fusion is an internal phenomena whereas scattering and other distant, less absorptive direct reaction mechanisms are responsible for the surface occurrence. We should note that for a given system, there may be many sets of possible Woods-Saxon parameters that describe elastic scattering data in a manner that is comparable. Since elastic scattering is a surface phenomenon, all sets of potential parameter sets produce Coulomb barriers with the same height V_B and fixed radial position R_B, but different sets produce different depths and slopes of effective potential of interior portion $r < R_B$. However, the fusion is an internal event that is defined by absorption in this area, and the values of the radius parameter R_{fus}, which is located in the region $0<r<R_B$, are responsible for the corresponding cross-section. The value of R_{fus}will be determined by a set of suitable parameters employed in the study. Therefore, it may have different values for different sets of potential. We do not need to alter the value of R_{fus} as a function of energy for study of σ_{fus} at various incidence energies as we have chosen a single potential for the description of both the fusion and elastic cross-sections. R_{fus}'s energy-independent character is essential since it makes the product $E_{c.m}\ \sigma_{fus}$ in the result of $d^2(E_{c.m}\ \sigma_{fus})/dE^2$, which is described in the next section.

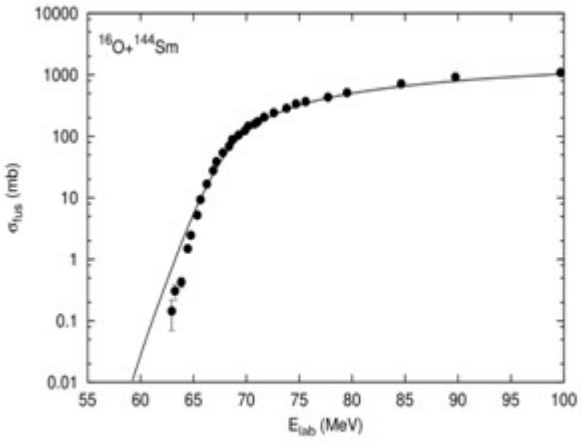

Figure 11: Variation offusion cross section σ_{fus}asafunction of energy E_{lab} forthe$^{16}O+^{144}$ Smsystem. He full curve represent sourcalculate dresults.The experimental data shown by solid circle sare obtained from [9].

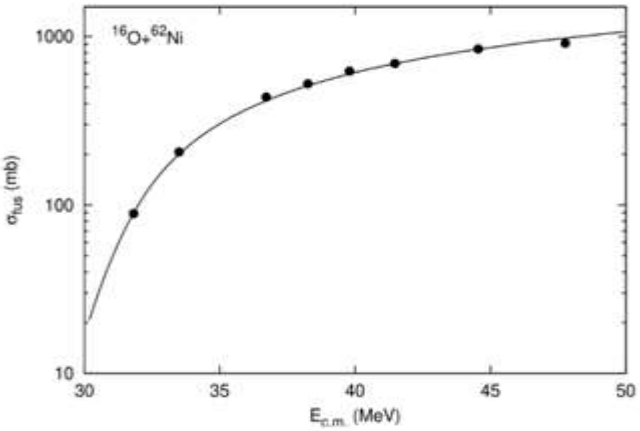

Figure 12: Variation of fusion cross section σ_{fus}as a function of energy $E_{c.m.}$for the $^{16}O+^{62}Ni$ system.The full curve represents our calculatedresult. The experim ental datashown by solid circle sare obtain edfrom [11].

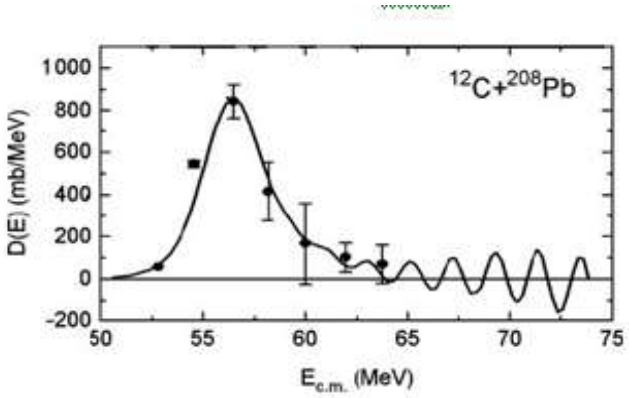

Figure 13: Variation of $D(E_{c.m}) = \frac{d^2(E_{c.m}.\sigma_{fus})}{dE_{c.m}^2}$ against energy $E_{c.m}$ for the results of for $^{12}C+^{208}Pb$ system. The full curves represent our calculated results. The experimental data shown by solid dots are obtained from [3].

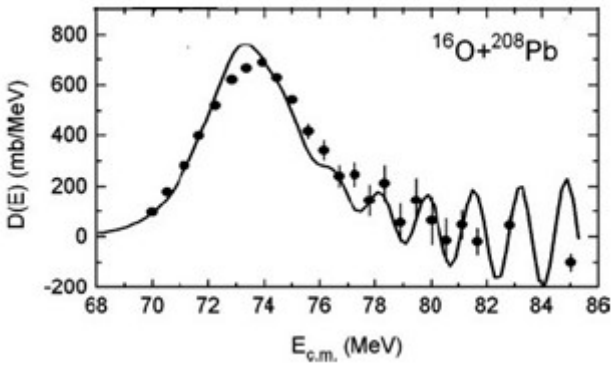

Figure 14: Variation of $D(E_{c.m}) = \frac{d^2(E_{c.m}.\sigma_{fus})}{dE_{c.m}^2}$against energy $E_{c.m}$ for the results of $^{16}O+^{208}$ for $^{16}O+^{208}$ Pbsystem. The full curves represent our calculated results. The experimental data shown by solid dots are obtained from [4].

3. **Explanation of D($E_{c.m.}$):** Fig.8 to Fig.12 show the values of σ_{fus} which are obtained from experiment and theory against energy. They do not exhibit any kind of structure. Therefore, nothing further can be inferred about the potential physical incidents that could be contributing to the fusion process from this logical interpretation of the monotonically evolving data. The identical result of σ_{fus} is reported in a different way as follows in order to provide some insight into these processes. One can extract values of a quantity that is the second derivative of the product $E_{c.m}$ σ_{fus} denoted by $\boldsymbol{D(E_{c.m})} = \frac{\boldsymbol{d^2(E_{c.m}.\sigma_{fus})}}{\boldsymbol{dE^2_{c.m}}}$ with respect to $E_{c.m}$. Thus, the point difference formula is given by

$$D(E) = [(E - \Delta E)\sigma_- - 2E\sigma + (E + \Delta E)\sigma_+]/(\Delta E)^2 \quad (35)$$

Where σ_- , σ and σ_+ indicate fusion cross sections σ_{fus} at centre of mass energies E – ΔE, E and E + ΔE, respectively with energy step size ΔE. The function D ($E_{c.m}$) is referred to as barrier distribution function [5, 9, 43].We get the amount $D(E_{c.m.})$ against energy $E_{c.m.}$ from our computed results of σ_{fus} using the formula (1.35). For the $^{12}C+^{208}Pb$ system, we present our results in Fig. 13 as a solid curve and then compare them with the relevant experimental data(solid circles). It can be observed that our calculation accurately reproduces the major peak as well as a few other minor peaks in the higher energy range.

Similarly, in Figs. 14, 16, and 17 we remarkably explain high oscillatory structures of the experimental data of $D(E_{c.m.})$ in $^{16}O+^{208}Pb$, $^{19}F+^{208}Pb$, $^{16}O+^{92}Zr$, $^{16}O+^{144}Sm$, $^{16}O+^{62}Ni$, and $^{6}Li+^{209}Bi$ systems.

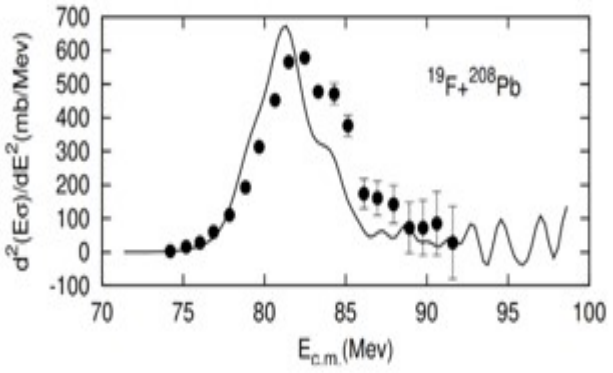

Figure 15: Variation of $D(E_{c.m}) = \frac{d^2(E_{c.m}.\sigma_{fus})}{dE^2_{c.m}}$ against energy $E_{c.m}$ for the results of $\sigma_{fus}$for $^{19}F+^{208}Pb$ system. The full curves represent our calculations. The experimental data shown by solid dots are by solid circles are obtained from [7].

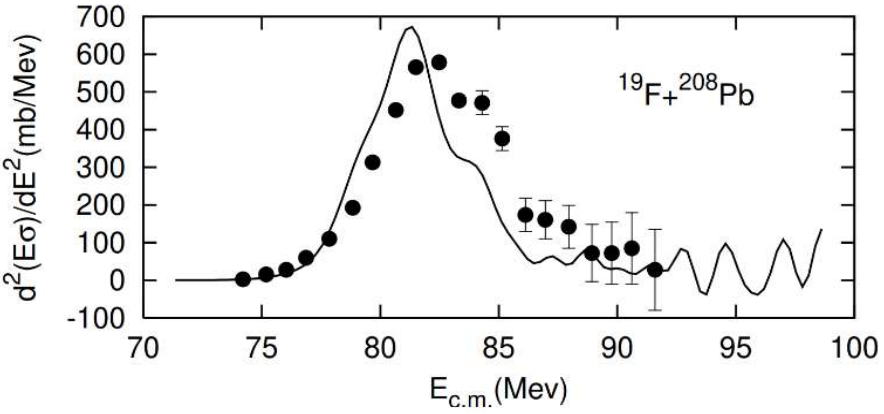

Figure 16 : Variation of $D(E)$ as a function of energy E_{lab} corresponding to results of σ_{fus} for $^{16}O+^{144}Sm$ system. The full curve represents our calculated result. The experimental data (solid circles) are obtained from [10].

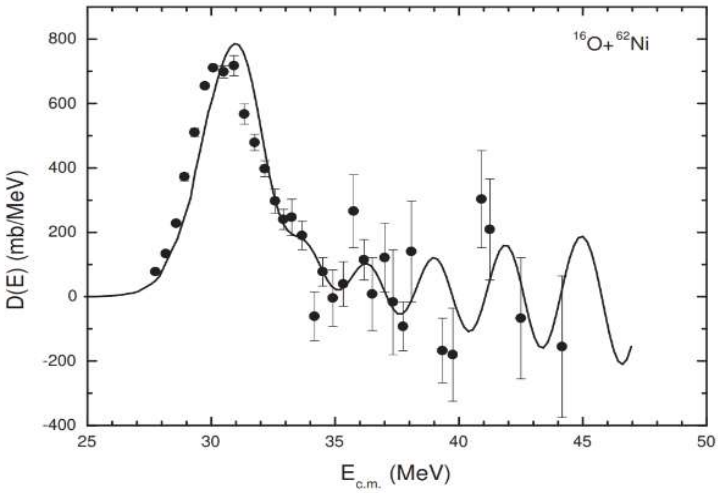

Figure 17: Variation of $D(E_{c.m}) = \frac{d^2(E_{c.m}.\sigma_{fus})}{dE^2_{c.m}}$ against energy $E_{c.m}$ for results of σ_{fus} for $^{16}O+^{62}Ni$system. The full curves represent our calculated results. The experimental data shown by solid dots are by solid circles are obtained from [7].

More crucially, the unfavourable character of some dips in the zone of higher-energy is fairly explained. The discovery [4] that the more microscopic CC calculation [44] for fusion has failed to explain the results of $D(E^{c.m}.)$ in the $16O+208_{Pb}$ system [4,23] raises the significance of this successful explanation. It's worth noting that there are three ways to disrupt the oscillatory structures in all of the systems mentioned above. The ways are as follows :

- By raising the value of the imaginary component W's strength,
- By taking into account a higher value of r^C, and
- By widening step size ΔE for the differentiation using formula (1.35).

In order to provide an appropriate explanation for the elastic scattering data as

well as an explanation for the observed results of cs σfus and D($E^{c.m}$.), when the values of W and r^C are fixed.

IV. SUMMARY AND CONCLUSION

Analytical solutions to the Schro¨dinger equation for the interaction of two nuclei with an optical potential of composite fashion result in a recursive mathematical formula for the scattering matrix. The formula (analytical) for the absorption cross-section has been established to take into consideration the reaction cross-section by using the same potential and wavefunction. The formulation is used for the colliding systems, namely, $12C+208_{Pb}$, $16O+208_{Pb}$, $19F+208_{Pb}$, $16O+144_{Sm}$, and $16O+62_{Ni}$ to analyze of the following experimental results consistently.

- Angular fluctuations of differential cross-sections of elastic scattering at various incident energies near the Coulomb barrier.
- Behaviour of cross-sections (σ^{fus}) of fusion against energy throughout a large range spanning Coulomb barrier area.
- Outcome of the distribution quantity $(E_{c.m}) = \frac{d^2(E_{c.m}.\sigma_{fus})}{dE_{c.m}^2}$.

The key characteristics that result from this analysis may be summed up as follows.

- Experimental data regarding elastic-scattering at various energies of projectile could be well explained by a single potential based on the format of Woods-Saxon potential without dependence on energy. The real part the complex potential considered should have larger depth, but smaller diffuseness, whereas, the imaginary part assumes weak strength for less absorption.
- A key component of the computation is the estimation of the reaction cross-sectional area that will be used for estimating fusion cross-sections by using the stepwise absorption approach. This procedure of dividing up the total cross-section is natural because neither the extraction process nor the division of the imaginary part ever requires additional energy.
- The results of cross-section σ_{fus} are presented in a form described as, $D(E_{c.m}) = \frac{d^2(E_{c.m}.\sigma_{fus})}{dE_{c.m}^2}$ by the technique of point difference formula. The new form shows peculiar peak structure when plotted against energy $E_{c.m}$. Our calculated outcomes for σfus presented in the aforementioned manner describe this outcome with highs and lows with a surprising degree of success.

- It has been found that resonance states can develop when two nuclei collide because of theoptical potential's weakly absorptive property indicated in item (a) above. Following that, it comes out that these resonances regulate the interesting oscillatory phenomena found in D(Ec.m.) mentioned in point (c).

REFERENCES

[1] S.Santra,P.Singh,S.Kailas,A.Chatterjee,A.Shrivastava,andK.Mahata,Phys.Rev.C64,024602(2001).
[2] F.Videbaek,R.B.Goldstein,L.Grodzins,S.G.Steadman,T.A.Belote,andJ.D.Garrett,Phys.Rev.15,954(1977).
[3] A.Mukherjee,D.J.Hinde,M.Dasgupta,K.Hagino,J.O.Newton,andR.D.Butt,Phys.Rev.C75,044608(2007).
[4] C.R.Morton,A.C.Berriman,M.Dasgupta,D.J.Hinde,J.O.Newton,K.Hagino,andI.J.Thompson,Phys.Rev.C6

0,044608(1999).
[5] M.Dasgupta,D.J.Hinde,N.Rowley,andA.M.Stefanini,Annu.Rev.Part.Sci.48,401(1998),andreferencestherei nC.J.Lin,J.C.Xu,H.Q.Zhang,Z.H.Liu,F.Yang,andL.X.Lu,Phys.Rev.C63064606(2001).
[6] D.J.Hinde,A.C.Berriman,M.Dasgupta,J.R.Leigh,J.C.Mein,C.R.Morton,andJ.O.Newton,Phys.Rev.C60054 602(1999).
[7] D. Abriola, D. DiGregorio, J. E. Testoni, A. Etchegoten, J. O. Fernandez, A. M. J. Ferrero, S. Gil, A. O. Macchiavelli, A. J.Pacheco,andJ.Kittl,Phys.Rev.C39546(1989).
[8] J.R.Leigh,M.Dasgupta,D.J.Hinde,J.C.Mein,C.R.Morton,R.C.Lemmon,J.P.Lestone,J.O.Newton,H.Timmers , J.X.Wei,andN.Rowley,Phys.Rev.C52,3151(1995).
[9] K.Hagino,N.Takigawa,andS.Kuyucak,Phys.Rev.Lett.792943(1997).
[10] N.Keeley,J.A.Christly,N.M.Clarke,B.R.Fulton,J.S.Lilley,M.A.Nagarajan,I.J.Thompson,Nucl.Phys.A5823 14(1995).
[11] N.Keeley,J.S.Lilley,J.X.Wei,M.Dasgupta,D.J.Hinde,J.R.Leigh,J.C.Mein,C.R.Morton,H.Timmers,andN.R owley,Nucl.Phys.A6281(1998).
[12] Y.EisenandZ.Vager,Nucl.Phys.A187,219(1972).
[13] T.Udagawa,B.T.Kim,andT.Tamura,Phys.Rev.C32,124(1985).
[14] T.Udagawa,S.-W.Hong,andT.Tamura,Phys.Rev.C32,1435(1985).
[15] J.R.BirkelundandJ.R.Huizenga,Annu.Rev.Nucl.Part.Sci.33,265(1983).
[16] S.G.SteadmanandM.J.Rhoades-Brown,Anuu.Rev.Nucl.Part.Sci.36,649(1986).
[17] G.R.Satchler,M.A.Nagarajan,J.S.Lilley,andI.J.Thompson,Phys.Rev.C41,1869(1990).
[18] M.A.NagarajanandG.R.Satchler,Phys.Lett.B173,29(1986).
[19] C.H.DassoandS.Landowne,Comput.Phys.Commun.46(1987)187;M.Dasgupta,A.Navin,Y.K.Agrawal,C.V .K.Baba,H.C.Jain,M.L.Thingan,andA.Roy,Nucl.Phys.A539,351(1992).
[20] I.J.Thompson,Comput.Phys.Rep.7,167(1998).
[21] K.Hagino,N.Rowley,andA.T.Kruppa,Comput.Phys.Commun.123,143(1999).
[22] HenningEsbensenandSerbanMisicu,Phys.Rev.C76,054609(2007).
[23] M.Dasgupta,D.J.Hinde,A.Diaz-Torres,B.Bouriquet,CatherineI.Low,G.J.Milburn,andJ.O.Newton,Pˆhys.Rev.Lett. 99,192701(2007).
[24] R.N.Sagaidak,S.P.Tretyakova,S.V.Khlebnikov,A.A.Ogloblin,N.Rowley,andW.H.Trzaska,Phys.Rev.C76, 034605(2007).
[25] J.O.Newton,R.D.Butt,M.Dasgupta,D.J.Hinde,I.I.Gontchar,C.R.Morton,andK.Hagino,Phys.Rev.C70,0246 05(2004).
[26] D.J.Hinde, M.Dasgupta, C.R.Morton, A.C. Berriman,R.D. Butt,andJ.O.Newton, Nucl.Phys.A654,864c (1999);D.J.Hinde,C.R.Morton,M.Dasgupta,J.R.Leigh,J.C.Mein,andH.Timmers,Nucl.Phys.A592,271(1995)
[27] M.R.Spinella,J.E.Testoni,O.Dragun,andH.D.Matra,Nucl.Phys.A687,385(2001).
[28] G.R.Satchler,M.A.Nagarajan,J.S.Lilley,andI.J.Thompson,Ann.Phys.178,110(1987).
[29] M.L.Halbert,J.R.Beene,D.C.Hensley,K.Honkanen,T.M.Semkow,V.Abenante,D.G.Sarantites,andZ.Li,Phys .Rev. C40,2558(1989).
[30] BasudebSahu,G.S.Mallick,B.B.Sahu,S.K.AgarwallaandC.S.Shastry,Phys.Rev.C77,024604(2008).
[31] R.R.Swain,C.Dash,P.Mohanty,B.B.SahuInt.J.Mod.E29,2050016(2020).
[32] C.Dash,R.R.Swain,G.Tripathy,I.Naik,B.B.Sahu.ChinesePhysicsC46,124104-1-8,(2022).
[33] R.H.LandauandM.J.P.Mejia,ComputationalPhysics(JohnWileyandSons,Newyork,1997).
[34] F.R.LoscalzoandT.D.Talbot,Bull.Amer.Math.Soc.73,438(1967).
[36] G.Micula,Math.Comp.27,807(1973).
[37] BasudebSahu,BidhubhusanSahu,andSantoshK.Agarwalla,Pramana:J.Phys.70(2007)27.
[38] M.A.Melkanoff,T.Sawada,andJ.Raynal,MethodsinComputationalPhysics,Vol.VI,NuclearOpticalModelC alculations(AcademicPress,NewYork,1966).
[39] C.S.ShastryandY.K.Gambhir,Phys.Rev.C28,1109(1983).
[40] M.P.Nicoli,F.Haas,R.M.Freeman,N.Aissaoui,C.Beck,A.Elanique,R.Nouicer,A.Morsad,S.Szilner,Z.Basra k,M.E.Brandan,andG.R.Satchler,Phys.Rev.C60,064608(1999).
[41] S.C.Pieper,M.J.Rhoades-Brown,andS.Landowne,Phys.Lett.B162,43(1985).
[42] R.M.DevriesandM.R.Clover,Nucl.Phys.A243,528(1975).
[43] A.B.BalantekinandN.Takigawa,Rev.Mod.Phys.70,77(1998).
[44] N.Rowley,G.R.Satchler,andP.H.Stelson,Phys.Lett.B254,25(1991).
[45] B.Sahu,L.Satpathy,andC.S.Shastry,Phys.Lett.A303,105(2002).
[46] B.Sahu,S.K.Agarwalla,andC.S.Shastry,Nucl.Phys.A713,45(2003).

